Optical Materials 147 (2024) 114631

Contents lists available at ScienceDirect

Optical Materials

journal homepage: www.elsevier.com/locate/optmat

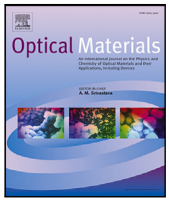

Research article

Polarization-independent hollow nanocuboid metasurfaces with robust quasi-bound states in the continuum

J.F. Algorri [a,b,c], V. Dmitriev [d], H.E. Hernández-Figueroa [e], L. Rodríguez-Cobo [b], F. Dell'Olio [f], A. Cusano [g], J.M. López-Higuera [a,b,c], D.C. Zografopoulos [h,*]

[a] Photonics Engineering Group, University of Cantabria, Santander, 39005, Spain
[b] CIBER de Bioingeniería, Biomateriales y Nanomedicina, Instituto de Salud Carlos III, Madrid, 28029, Spain
[c] Instituto de Investigación Sanitaria Valdecilla (IDIVAL), Santander, 39011, Spain
[d] Electrical Engineering Department, Federal University of Pará, PO Box 8619, Agencia UFPA, Belém, 66075-900, Brazil
[e] School of Electrical and Computer Engineering, University of Campinas-UNICAMP, Campinas, 13083-852, Brazil
[f] Department of Electrical and Information Engineering, Polytecnic University of Bari, Bari, 70125, Italy
[g] Department of Engineering, University of Sannio, Benevento, 82100, Italy
[h] Consiglio Nazionale delle Ricerche, Istituto per la Microelettronica e Microsistemi, Via del fosso del cavaliere 100, Rome, 00133, Italy

ARTICLE INFO

Keywords:
Dielectric metasurfaces
Biosensing
Bound states in the continuum
Fano resonances
Field enhancement
Refractometry

ABSTRACT

All-dielectric metasurfaces supporting resonant quasi-bound states in the continuum (qBIC) offer an ideal platform for various applications relying on intense light–matter interaction in highly localized and enhanced fields. Here, we propose a dielectric metasurface composed of hollow GaP nanocuboid quadrumers periodically arranged on a silica substrate. The metasurface supports a qBIC resonant mode with an antiferroelectric field configuration, which is very robust to large perturbations of the cuboid structure thanks to its perpendicular electric dipole field profile. The perturbed quadrumer arrangement retains C_{4v} symmetry, thus allowing for polarization-independent optical response for normally incident planewaves. In addition, the resonant mode dispersion is investigated, revealing interesting features, such as low birefringence along the ΓM contour of the Brillouin zone and very low dispersion for the TM polarization along the ΓX direction. The metasurface is designed to resonate close to 785 nm, which is highly relevant for Raman spectroscopy, leveraging the strong field enhancement at the interface with the overlayer material. Moreover, its performance as a bulk refractometric sensor is discussed. The proposed dielectric metasurface is promising for emerging photonic phenomena where strong light–matter interaction plays a key role.

1. Introduction

Optical sensing techniques are crucial in various fields such as biomedicine, material science, and environmental monitoring due to their fast and robust ability to detect and differentiate target objects from diverse samples. Recently, nanophotonic metasurfaces have emerged as a promising platform to enhance sensing technologies [1]. These are artificial photonic devices made up of subwavelength nanoresonators and their functionalities can be customized by manipulating their geometric parameters [2]. For optical sensing, their ability to concentrate light into nanoscale electromagnetic hotspots has been utilized to boost the sensitivity of different detection techniques. On the other hand, vibrational spectroscopy based on nanophotonics, such as surface enhanced Raman spectroscopy (SERS), offers an alternative method to refractometric detection for biomolecular sensing [3]. In particular, it provides chemically specific information about each analyte and facilitates label-free sensing and monitoring of chemical reactions and interaction kinetics between various analytes.

For a long time, the domain of metasurfaces was dominated by plasmonic materials due to their ability to support localized surface plasmon resonances [4], which results in strong, subwavelength concentration of the electric field around the plasmonic particles/oligomers [5,6], or in deeply subwavelength resonant cavities [7]. This feature is particularly useful for applications such as refractometric sensing and SERS, where the enhanced electromagnetic field at the metasurface interface with the external medium significantly improves the signal strength. However, plasmonic metasurfaces suffer from substantial ohmic losses, which limit the quality factor (Q-factor) [8] and hence

* Corresponding author.
E-mail address: dimitrios.zografopoulos@artov.imm.cnr.it (D.C. Zografopoulos).

https://doi.org/10.1016/j.optmat.2023.114631
Received 5 October 2023; Received in revised form 8 November 2023; Accepted 22 November 2023

the sensor's figure of merit (FoM) [9]. In addition, such ohmic losses lead to local heating, which can damage the biological analyte in the case of biosensing.

To tackle such issues, dielectric metasurfaces have emerged as a promising alternative, offering high Q-factor and low ohmic losses, thanks to their ability to support electric and magnetic Mie-type resonances [10]. These resonances occur when the incident light excites electric and magnetic multipoles inside the dielectric particles, leading to an optical response, which exhibits similarities to localized surface plasmons in their far field optical behavior. By exploiting the symmetries of the periodic metasurface structure, Mie-type resonances can be of dark nature, also known as bound states in the continuum (BIC), and hence not externally accessible. However, they can manifest as quasi-BIC (qBIC) by perturbing the metasurface symmetry and offer control over the radiative Q-factor value, which asymptotically diverges to infinity. Thanks to the high Q-factors and the associated strong field confinement, BIC metasurfaces have emerged as a platform for an abundance of applications based on strongly resonant light manipulation. Some examples include the enhancement of nonlinear phenomena, such as higher harmonic generation, light emission and lasing with scalable emission volume and high Purcell factor, biosensing, narrowband dichroism in chiral configurations, and narrowband super absorption [11,12]. Although BIC can manifest in both metallic and dielectric metasurfaces, the former being a promising platform for, e.g., THz applications where losses in metallic resonators are tolerable [13,14], in the infrared or visible spectrum dielectric transparent materials are needed in order to experimentally observe strong BIC resonances.

Unlike plasmonic resonances, Mie-type resonances tend to confine the electric field enhancement inside the dielectric resonators, limiting their effectiveness in applications requiring strong light interaction with the surrounding environment, as in sensing [15]. However, the collective oscillations that manifest in periodic metasurfaces provide a means of engineering the resonant mode profile, enabling also delocalized field profiles. That said, specially engineered dielectric nanostructures have been recently employed for refractometric label-free sensing. For instance, a Si nanodisk metasurface was used to detect streptavidin down to 5 ng/mL when the surface was covered with biotin molecules [16]. Later developments integrated these Si nanodisks with microfluidics, optimizing them for near-IR wavelengths, and allowed for the detection of substances like the prostate-specific antigen (PSA), with a limit of detection (LOD) down to 0.69 ng/mL of PSA [17]. Recent research utilized large-area imaging configurations with high-Q qBIC metasurfaces [18,19]. They demonstrated the use of a 2D array of pixelated metasurfaces, with each metapixel tuned to a specific resonant frequency. This allowed access to molecular signals across an extended wavelength range with high sensitivity and negated the need for costly spectroscopic equipment. Other experimental works demonstrated bulk refractometry in qBIC metasurfaces with sensitivity values of a few hundreds nm/RIU and Q-factors in the same range of values [20–23].

In the case of SERS less progress has been registered. For example, Caldarola et al. demonstrated an application using a metasurface built from a silicon dimer array on a silicon-on-insulator substrate [24]. This metasurface was utilized for SERS to identify a thin layer of polymethylmethacrylate applied onto the metasurface. In another example, a similar silicon dimer metasurface was fabricated on a sapphire substrate to detect a self-assembled monolayer of β-carotene molecules [25]. By exploiting qBIC in a silicon nitride nanohole metasurface, Romano et al. demonstrated an enhancement factor of the Raman signal above 1000 [26].

However, despite the promising prospects, realizing dielectric metasurfaces with stable, high Q-factor resonances and field localization outside or at the interface of the resonator volume presents still significant challenges. Fabricated metasurfaces inevitably suffer from resonance broadening due to several factors, some of the most important of which are fabrication tolerances, non-perfect illumination conditions and the finite metasurface size, thus limiting the maximum measurable Q-factor [27,28]. Therefore, it is important to combine the desired resonant field properties with increased robustness of the resonators in terms of statistical fabrication deviations from the nominal design. In this context, some particular techniques towards robust qBIC resonances are the concepts of merging BIC with opposite topological charges [29] or band engineering leading to folding-induced BIC in the Brillouin zone [30].

In this work, we propose a metasurface whose constituent element is a hollow GaP nanocuboid, in which the hole is diagonally displaced from the cuboid center. By arranging the cuboids in periodic quadrumer clusters on a silica substrate, one achieves both control over the radiative Q-factor of the resonant qBIC mode and polarization-independent operation [31–33]. Although similar geometries have been investigated in the literature as strongly resonant metasurfaces based on toroidal [34–37] or magnetic dipole modes [38,39], here we investigate a qBIC antisymmetric supermode characterized by a perpendicular electric dipole moment. This particular field configuration provides very high robustness of the qBIC mode to perturbations of the cuboid geometry even when the hole is displaced at the cuboid corner and occupies significant part of its volume. The metasurface is designed so that it operates in the vicinity of 785 nm, which is a standard laser wavelength employed in Raman spectroscopy.

The study initially explores the symmetry properties of the metasurface using group theory analysis. Subsequently, the investigation focuses on the fundamental optical characteristics of the antiferroelectric qBIC resonance, utilizing techniques such as finite-element eigenfrequency and full-wave simulations. The dependence of the resonant wavelengths and Q-factors in response to symmetry perturbations is evaluated, demonstrating the robustness of the qBIC mode and high Q-values above 10^5 in the entire parametric space. In addition, the band diagram of the mode is calculated, studying the modal birefringence in the case of oblique incidence and revealing very low dispersion for the TM polarization along the ΓX direction. Such almost flat dispersion is of paramount importance in terms of maximizing the experimentally achievable Q-factors, as it mitigates resonance broadening effects. Finally, the sensitivity of the metasurface for refractometry is evaluated as a function of the analyte index, demonstrating high values which, combined with the high Q-factors, are promising for sensors with very high FoM and low LOD. Overall, the metasurface meets the requirements for applications based on strong light–matter interaction, such as refractometric sensing and Raman spectroscopy, providing a simple design with high robustness to fabrication tolerances.

2. Results

2.1. Geometry and materials

The layout of the investigated dielectric metasurface is depicted in Fig. 1(a) and it is composed of an array of GaP hollow nanocuboids periodically arranged on a glass (SiO_2) substrate. The fabrication of the proposed metasurface can be achieved by standard nanofabrication protocols, namely: (i) growth of a thin GaP layer of thickness h = 129 nm on the substrate, for instance, by RF sputtering [40], (ii) definition of the metasurface pattern through electron-beam lithography, and (iii) fabrication of the periodic array of GaP elements through inductive coupled plasma etching. Using this procedure, GaP metasurfaces with features of similar dimensions have been experimentally demonstrated [41,42]. As shown in the unit cell definition of Fig. 1(b), the GaP cuboids are characterized by a square cross-section of size w_c = 127 nm. The distance between adjacent cuboids is $d = w_c$, such that the metasurface pitch is $p = 4w_c$. In each cuboid there is a square hole of size w_h, whose center is displaced with respect to the cuboid center along the diagonal at a distance s, as in Fig. 1(b). Furthermore, we define two dimensionless perturbation factors, which

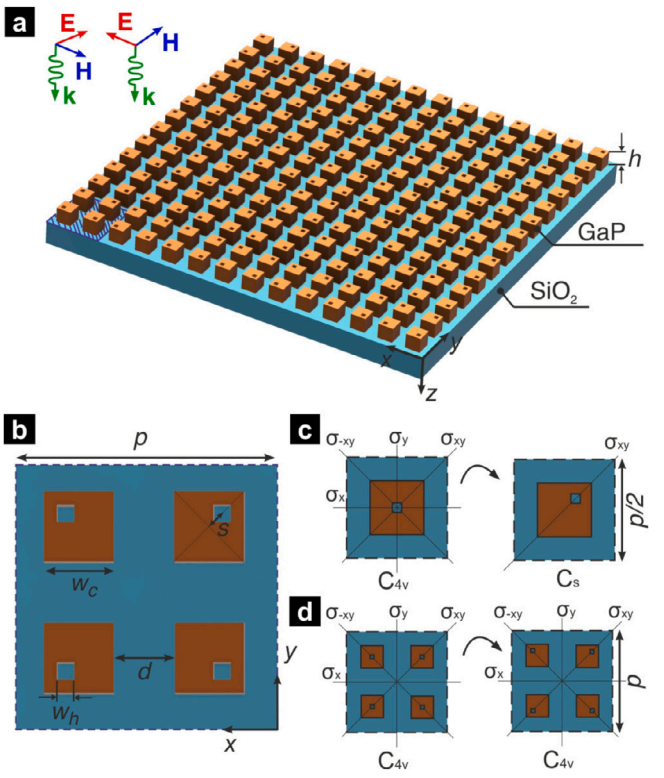

Fig. 1. (a) Three-dimensional schematic view of the investigated metasurface composed of GaP hollow cuboids on a SiO_2 substrate. The metasurface response is polarization-insensitive for normally incident planewaves. The shaded surface in the bottom left corner denotes the metasurface unit cell. (b) Definition of the geometrical parameters of the unit cell. (c) Symmetry group and its elements of a single-cuboid unit cell with a square hole in the cuboid center and diagonally shifted. (d) Symmetry group and its elements of the metasurface four-cuboid unit cell. The cell maintains its C_{4v} symmetry when the hole centers are displaced along the diagonals.

describe the relative deviation of the hollow cuboid with respect to its solid counterpart: $q_h = w_h/w_c$ and $q_s = \sqrt{2}s/(w_c - w_h)$. In the limit cases of $q_h = 1$ and $q_s = 1$ the cuboid vanishes or, respectively, removes one corner of the cuboid.

The metasurface is designed such that the target BIC resonance occurs in the vicinity of $\lambda_0 = 785$ nm, which is a standard wavelength used in Raman spectroscopy, offering a good trade-off between high intensity and low fluorescence compared to the Raman working wavelengths of 1064 and 532 nm, respectively. The refractive indices for GaP and SiO_2 at λ_0 are $n_{GaP} = 3.203$ and $n_g = 1.454$, and their frequency dispersion was taken into account in the following study [43,44]. Both materials were considered lossless in the analysis, as their extinction coefficient is negligible in the spectral window around the target wavelength. The dielectric properties of GaP, namely high refractive index and negligible absorption losses, justify its selection for the design of the investigated metasurface. The high index allows for subwavelength resonators and metasurface unit cells, thus avoiding diffraction, and high transparency, which is essential for achieving high Q-values. Although in a real system other loss mechanisms may be present, e.g., scattering losses from fabrication imperfections, such effects are not investigated in this work.

2.2. Symmetry analysis

As a first step in the investigation of the proposed metasurface, we apply group theory to its symmetry analysis. The metasurface structure possesses a certain symmetry in the xOy plane, while it does not have any horizontal plane of symmetry $z = \text{const}$. Therefore we shall consider a 2D problem. In order to simplify our description by the group-theoretical method, we consider two levels of the problem:

1. the first (lower) level: an array with one cuboid in the unit cell,
2. the second (higher) level: an array of quadrumers with four cuboids in the unit cell.

2.2.1. Single cuboid unit cell

The symmetry of a cuboid placed in the center of a square unit cell with pitch $p' = p/2$, as shown in Fig. 1(c), is described in the xOy plane by the group C_{4v} (in Schoenflies notations [45]). It is noted that the group C_{4v} contains also the rotations C_2 and C_4, which are not shown in Fig. 1(c) as they are not relevant in the frame of the present analysis. When a square hole is introduced in the cuboid and the z-axes of the cuboid and the hole coincide, the symmetry C_{4v} of the cuboid is preserved. However, if the position of the hole is shifted along one of the diagonals, the symmetry of the cuboid is reduced to the group C_s with only one plane of symmetry σ_{xy}, as in Fig. 1(c).

Now we apply to the problem of excitation of the investigated mode, which is an electric dipole mode with the moment $\mathbf{p}_z$ oriented along the axis z. It is convenient to discuss the excitation of the cuboid in terms of the magnetic field. The field profile of the mode was calculated by an eigenfrequency study using the finite-element method (FEM) implemented in COMSOL Multiphysics™. The unit cell of the metasurface was simulated by properly applying periodic boundary conditions at the lateral walls and a perfectly matched layer combined with scattering boundary conditions at the top and bottom of the computational domain. Unless mentioned otherwise, eigenfrequency simulations in this study were performed at the Γ point, which corresponds to normally incident planewaves. It is also remarked that the mild dielectric dispersion of the studied media (GaP and SiO_2) was taken into account, as the COMSOL eigenfrequency solver transforms nonlinear eigenvalue problems to linear ones by performing a second-order Taylor expansion of the material parameters around the target wavelength. The maximum size of the mesh elements was ten times less than the wavelength in the corresponding media and the minimum size was selected five times smaller than the width of the nanoholes, which are the smallest geometrical features of the metasurface.

The results, presented in Fig. 2, show that the in-plane electric field is very weak, with some higher intensity only at the outer corner edges of the cuboid, while the out-of-plane E_z component is dominant, indicating a dipole mode with moment $\mathbf{p}_z$. This is further verified by the structure of the magnetic field, which is visualized by the arrow plot in Fig. 2. The magnetic field in the xOy plane is almost circular, slightly deformed by the square geometry of the cuboid.

In the symmetry C_{4v}, the circular field $\mathbf{H}_{xy}$ is described by the 1D IRREP (irreducible representation) A_2 (see, e.g., Table 2 in [46]). However, the field $\mathbf{H}^{inc}$ of the incident wave belongs to the 2D IRREP E. Therefore, the $\mathbf{H}_{xy}$ and $\mathbf{H}^{inc}$ fields belong to different IRREPs and in the symmetry C_{4v}, assuming a normally incident plane wave, the investigated electric dipole mode is dark (pure BIC). If the symmetry of the cuboid is reduced to C_s by introducing a hole the excitation is possible when $\mathbf{H}^{inc}$ is not parallel to the diagonal of the hole dislocation, which defines the symmetry plane σ_{xy}.

2.2.2. Cuboid cluster unit cell

Next, we consider a quadrumer, where the unit cell of the array consists of four cuboids. The individual cuboids with reduced symmetry C_s are arranged in a square cell with their planes of symmetry, oriented along the diagonals of the cell square, as shown in Fig. 1(d). Thus, in this structure the C_{4v} symmetry of the quadrumer is preserved, regardless of the displacement of the cuboid center. However, the dimensions of the first Brillouin zone of the quadrumer are reduced by half in comparison with those of the case with one cuboid in the unit cell. Due to preservation of the symmetry C_{4v}, the array possesses polarization independence of the excitation of the dipole mode in

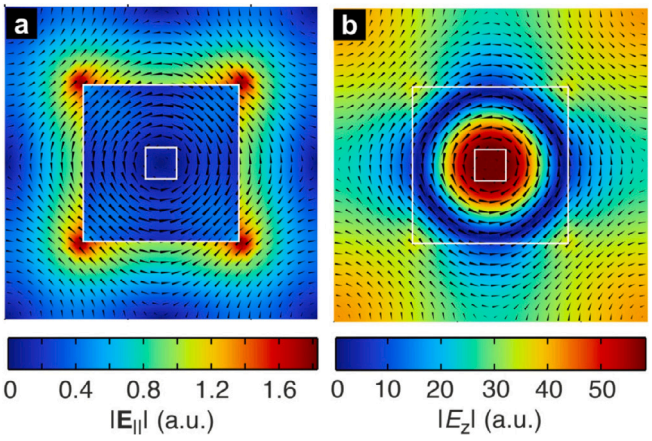

Fig. 2. Field structures for the investigated electric dipole mode in a metasurface with a single cuboid unit cell ($q_h = 0.2$): magnitude of the (a) in-plane and (b) out-of-plane electric eigenfield vector. The arrow plot in both cases shows the distribution of the in-plane magnetic field.

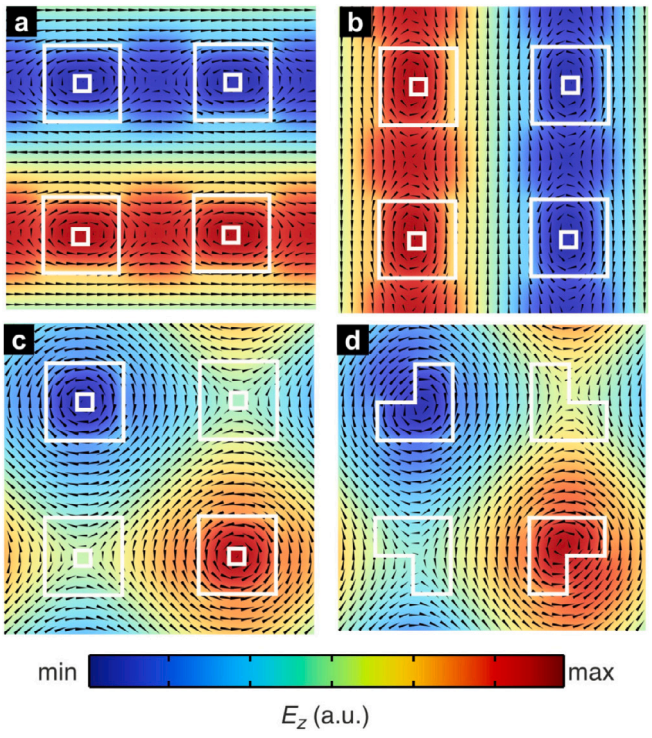

Fig. 3. Field structure of the E_z eigenfield component and the in-plane magnetic field (arrow plot) of the investigated supermode in a metasurface with cuboid cluster unit cell, which can be excited by a linearly polarized magnetic field $\mathbf{H}^{inc}$: (a) y-polarized excitation ($q_h = 0.2$, $q_s = 0$), (b) x-polarized excitation ($q_h = 0.2$, $q_s = 0$), (c) xy-polarized excitation ($q_h = 0.2$, $q_s = 0$), and (d) xy-polarized excitation ($q_h = 0.5$, $q_s = 1$). In all cases the antiferroelectric-like order of the electric field is observed. Blue (red) color corresponds to negative (positive) values of E_z.

cuboids. Nevertheless, the structure of the field in the unit cell depends on the polarization of the incident wave.

Now we apply to the description of fields in the unit cell with four cuboids. The eigensolutions in case of the IRREP E are fields $\mathbf{H}_x$ and $\mathbf{H}_y$. These fields correspond to the excitation by $\mathbf{H}_x^{inc}$ or $\mathbf{H}_y^{inc}$, respectively. In both these cases the field $\mathbf{H}^{inc}$ is oriented with 45° with respect to the (diagonal) planes of symmetry of the cuboids, and all of the four cuboids are excited equally. This is confirmed by the eigenfields shown in Fig. 3(a) and (b), which show the E_z profile for the investigated electric dipole mode, corresponding to $\mathbf{H}_y^{inc}$ and $\mathbf{H}_x^{inc}$ excitation, respectively. All four cuboids are equally excited, however the sign of E_z shows an anti-symmetric configuration, indicating an inversion of the dipole moment $\mathbf{p}_z$ direction, in what can be termed as antiferroelectric order. In general, mode hybridization in metasurfaces of resonator clusters can lead to supermodes with peculiar field profile characteristics, such as ferromagnetic or antiferromagnetic order [47, 48].

Any linear combination of the fields $\mathbf{H}_x$ and $\mathbf{H}_y$ is also an eigensolution of the system with the same eigenvalue and it can be excited by the corresponding $\mathbf{H}^{inc}$. In a particular case when the incident field $\mathbf{H}^{inc}$ is oriented along one of the unit cell diagonals, only two of the four cuboids will be excited. This is demonstrated in the E_z profile shown Fig. 3(c), calculated for a 45°, or $\mathbf{H}_{xy}^{inc}$, polarization. Notice, that the symmetry analysis can be fulfilled also in terms of electric field $\mathbf{E}^{inc}$ of incident wave, interchanging the corresponding subindices, for example, instead of $\mathbf{H}_x^{inc}$ one should use $\mathbf{E}_y^{inc}$.

The vertical electric dipole nature of the investigated supermode provides increased robustness of the field profile under the perturbation induced by the presence of the displaced holes. Since both the in-plane electric field components are weak, the high-index contrast hole/GaP interfaces do not give rise to strong electric field discontinuities. This is contrary to similar structures with strong in-plane electric fields, such as silicon slot waveguides, where the field component perpendicular to the interface undergoes a discontinuity proportional to the ratio of the permittivities of the two adjacent materials leading to strong field confinement in the low-index material [49].

A demonstration of the mode robustness is provided in Fig. 3(d), which shows the eigenfield of a perturbed quadrumer cuboid structure, where the hole occupies 25% of the cuboid volume ($q_h = 0.5$) and is placed in the corner of the cuboid ($q_s = 1$). Although the cuboid geometry is radically modified, the electric and magnetic eigenfields do not deviate significantly from those calculated in Fig. 3(c). This implies that the structure is indeed robust to geometrical perturbations. The electromagnetic properties of the investigated qBIC supermode, namely resonant wavelength and Q-factor, are accordingly affected, as it will be discussed next.

2.3. Properties of the qBIC antiferroelectric resonance

The investigated antisymmetric mode is a pure BIC when the holes are situated at the cuboid centers ($q_s = 0$). In case they are displaced, the BIC mode becomes qBIC with a finite radiative Q-factor and it can be excited as discussed in the previous Section. Fig. 4 investigates the resonant wavelength λ_0 and the Q-factor variation of the qBIC mode for two scenarios: a fixed hole size of $q_h = 0.2$ and $0 \le q_s \le 1$ and a fixed displacement $q_s = 1$ and $0 \le q_h \le 0.5$.

Fig. 4(a) shows that the dependence of λ_0 on q_s is very low, with an overall change in λ_0 lower than 2 nm. The introduction of a hole with $q_h = 0.2$ induces a negligible variation in the electric field profile, as already stressed in the discussion of Fig. 3. This is also reflected in the results of Fig. 4(b), where, although the increase of q_s does reduce the Q-factor, the values of the latter remain above 10^6 up to $q_s = 1$. On the contrary, the increase of the hole size situated at the cuboid corner ($q_s = 1$) produces a more radical change of the cuboid geometry, thus leading to higher variations of λ_0 and Q-factor with respect to the first scenario. Still, the Q-factor remains high also in this case ($Q > 10^5$). In both cases, the $Q(q_s, q_h)$ curve follows the inverse quadratic law in the low perturbation regime, which is typical of non-diffracting qBIC metasurfaces [50]. The Q-factors of Fig. 4(b) were calculated by applying the formula $Q = \Re(\tilde{\omega})/2\Im(\tilde{\omega})$, where $\tilde{\omega}$ are the complex eigenfrequencies derived from FEM simulations.

The transmittance spectra for three values of q_s and $q_h = 0.2$ were calculated by means of full-wave FEM simulations and they are presented in Fig. 4(c). The normally impinging planewave was excited

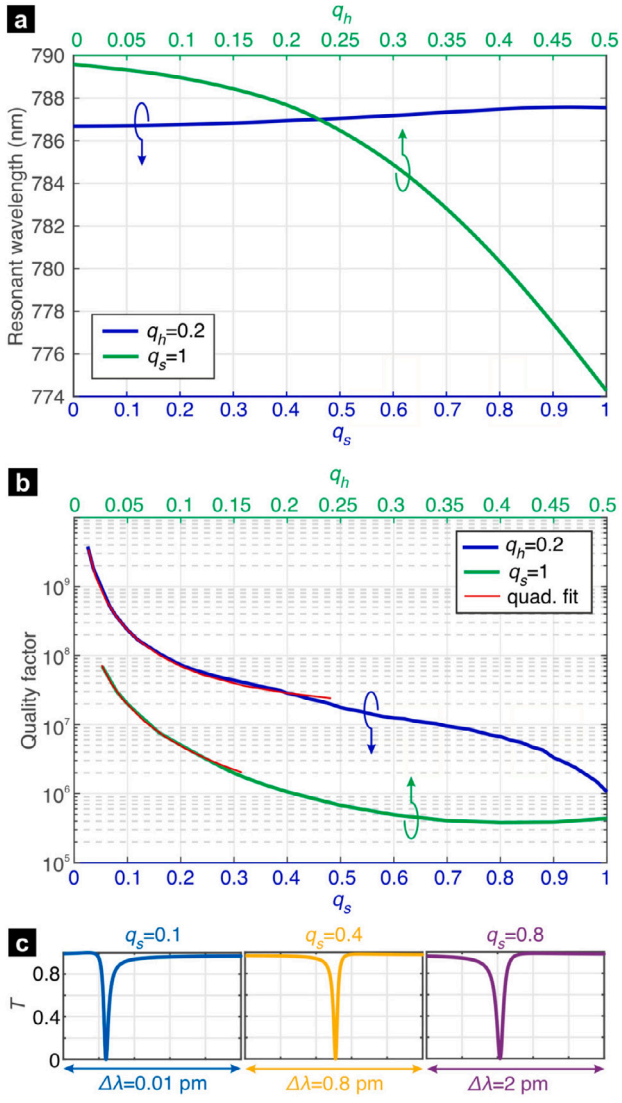

Fig. 4. Variation of (a) the resonant wavelength and (b) the Q-factor of the supermode for two scenarios: $q_h = 0.2$, $0 \le q_s \le 1$ and $q_s = 1$, $0 \le q_h \le 0.5$. (c) Transmittance spectra of the metasurface calculated for $q_h = 0.2$ and three values of q_s.

by defining a port boundary condition at a plane above the metasurface and transmittance was recorded at a symmetrically placed port in the substrate, with reference to Fig. 1(a). The resonances manifest as strong dips resembling a notch filter and the Fano profile of the resonant spectra is almost Lorentzian. The linewidths correspond to the eigenfrequency results of Fig. 4(b), with a Q-factor of approximately 10^8 for the $q_s = 0.1$ case. It is reminded that these values refer to the radiative Q-factor; the maximum experimentally measurable value is limited by non-radiative loss mechanisms, as it will be discussed. The closest other resonant modes of the metasurface are spectrally separated by several nanometers and, hence, do not interfere with the investigated qBIC resonance.

2.4. Dispersion analysis

The resonant response of the qBIC supermode is polarization-independent in the case of a normally incident planewave. In the case of oblique incidence, the symmetry of the structure breaks and the two linear polarizations are no longer degenerate. In addition, the resonant wavelength changes, which is a major factor that induces resonance

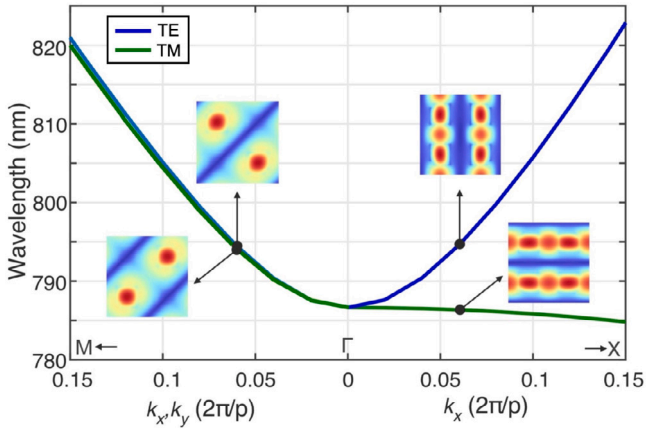

Fig. 5. Band diagram of the investigated supermode along the ΓX and ΓM contour of the irreducible Brillouin zone. For oblique incidence (off-Γ point) the band splits in two branches corresponding to different polarization. The insets show the norm of the electric field calculated at $\{k_x = 0.06,\ k_y = 0\}$ and $\{k_x = 0.06,\ k_y = 0.06\}$ in units of $(2\pi/p)$.

broadening in experimentally studied qBIC metasurfaces due to the $\lambda_0(k)$ dispersion [27].

To evaluate such effects, the band diagram of the qBIC mode corresponding to $q_h = 0.2$ and $q_s = 1$ was calculated by eigenfrequency analysis along the ΓX and ΓM contours of the irreducible Brillouin zone of the quadrumer metasurface. The results are presented in Fig. 5, where the insets show the norm of the electric eigenfield calculated at $\{k_x = 0.06,\ k_y = 0\}$ and $\{k_x = 0.06,\ k_y = 0.06\}$ in units of $(2\pi/p)$ for both orthogonal polarizations. It is observed that in the ΓM direction, which corresponds to $k_x = k_y$, namely a plane of incidence along the diagonal of the unit cell, the two orthogonal supermodes have almost the same resonant wavelength and significant dispersion.

On the contrary, in the ΓX direction, namely xOz plane of incidence, the TE supermode shows strong dispersion, whereas the TM supermode the opposite. This property indicates that experimentally probing the investigated metasurface with a x-polarized beam would facilitate the measurement of high Q-factors, thanks to the low dispersion, which minimizes the resonance broadening stemming from factors such as the angular content of the probing beam or the finite metasurface size. In particular, the oblique k-vector components of a non-perfectly collimated beam excite resonances in the vicinity of the Γ-point. A similar effect, leading to k-vector spread, stems also from the finite metasurface size due to discretization of the Bloch mode continuum [11]. Low dispersion guarantees that the corresponding spread in the resonant wavelengths excited by these k-vectors and, consequently, the resonance broadening are minimized, thus maintaining high Q-factors [38]. Such strong resonances are key, for instance, to selective filtering, enhancement of nonlinear processes or to improve the FoM of refractometric sensors, as discussed below.

2.5. Refractometric sensing and SERS

Here, we investigate the performance of the proposed metasurface as a bulk refractometric sensor, where we consider that the analyte occupies the overlayer volume. The sensitivity S is calculated by the shift of λ_0 due to variations of the analyte index n_a, i.e. $S = \Delta\lambda_0/\Delta n_a$, as calculated by eigenfrequency analysis for various values of n_a for a metasurface with $q_h = 0.2$ and $q_s = 0$. In the case of index-matching, namely when $n_a = n_g$, the field distribution is symmetric, whereas for $n_a < n_g$ ($n_a > n_g$) the electric field leaks into the substrate (overlayer). Hence, the sensor's sensitivity increases with n_a, as verified in the results of Fig. 6, as the refractive index contrast between the overlayer and the metasurface drops and the resonant field extends

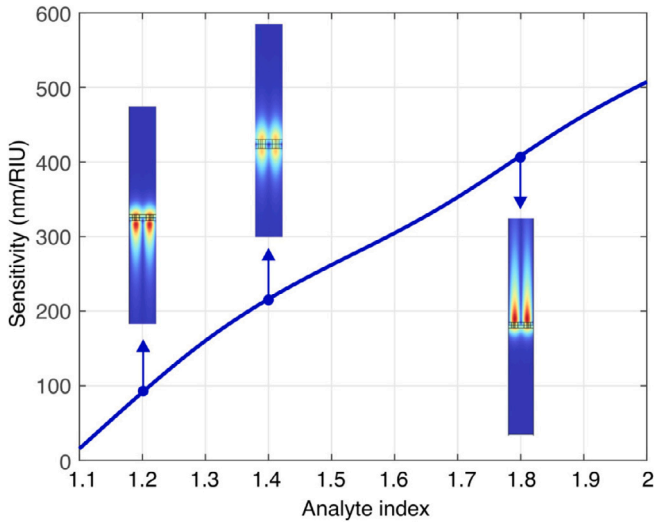

Fig. 6. Sensitivity calculated for $q_h = 0.2$ and $q_s = 0$ as a function of the analyte index n_a covering the overlayer of the metasurface. The insets show the norm of the resonant electric field for three values of n_a.

more into the overlayer region [51]. The sensitivity shows a quasi-linear dependence $S(n_a)$, with a value ~200 nm/RIU around $n_a = 1.35$, which increases up to 500 nm/RIU for $n_a = 2$. Such values are comparable with the state-of-the-art in qBIC refractometric sensors working close to 800 nm [19,52–54]. To facilitate or standardize the refractometric measurements, the metasurface can be bonded with a polydimethylsiloxane (PDMS) microfluidic chamber, which controls the analyte flow through inlet/outlet channels [52].

High sensitivity values, combined with the high Q-factors of the metasurface allow for refractometric sensing with high FoM and LOD [23,33]. The theoretically calculated FoM for the investigated sensor tends to infinity, as it is proportional to the Q-factor [33], whereas, in practice, it will be bound by the finite Q-factor due to non-radiative losses. In this context, the demonstrated robustness and low dispersion for the TM polarization can mitigate resonance broadening and increase the experimentally achievable Q-factor and FoM [27,28,38].

The improved sensitivity for higher values of n_a stems from the increased leakage of the resonant near field into the overlayer, as evidenced in the insets of Fig. 6, where the norm of the resonant field is plotted for $n_a = 1.2$, 1.4, and 1.8. To quantify this effect, the percentage of the total mode energy stored in the overlayer, namely the analyte, was calculated for the abovementioned values of n_a, found equal to 20%, 39%, 83%, respectively. The same effect can also be exploited in SERS, as for $n_a > n_g$ the maximum of the resonant electric field is located just above the metasurface/analyte interface. As an example, full-wave FEM simulations for a qBIC-resonant metasurface with $q_h = q_s = 0.2$ demonstrated a maximum field enhancement factor equal to 2500, 5000, 8000, calculated at a z-plane 100 nm above the metasurface for the three considered values of n_a. The range of suitable analyte indices for sensing and/or SERS can be expanded toward lower values by considering a substrate with lower refractive index compared to silica, for instance MgF_2 [55].

3. Conclusions

In conclusion, we have proposed and theoretically investigated a qBIC-resonant all-dielectric metasurface based on GaP quadrumer nanocuboid arrays on silica. The metasurface structure allows for polarization-independent operation for a normally incident planewave. The resonant qBIC supermode is characterized by an antiferroelectric field configuration, which provides very high robustness in terms of geometrical variations, thus increasing the metasurface tolerance to fabrication errors. Moreover, the dispersion analysis showed very low dispersion for the TM polarization, which further reduces the resonance broadening in realistic conditions. The resonant field shows very strong local confinement at a wavelength optimized for Raman spectroscopy. This could enhance the signal of the Raman scattered light, thus improving the detection of low-concentration analytes. The performance of the metasurface for refractometric sensing was evaluated, revealing sensitivity values in the order of a few 100s nm/RIU for typical analyte indices. This, in combination with high achievable Q-factors, makes it promising as a sensor with a very high figure of merit. Particularly, in biosensing applications, where small changes in the refractive index can indicate the presence of specific biomolecules. The high robustness of the qBIC supermode to geometrical variations increases the metasurface tolerance to fabrication errors, making the manufacturing process more feasible and cost-effective. The low dispersion for the TM polarization reduces resonance broadening, which is particularly beneficial in applications requiring a narrow resonance peak, such as in optical filters or lasers. In light of these findings, our BIC metasurface shows promising potential for real-world applications in areas such as Raman spectroscopy, refractometric sensing, and more.

CRediT authorship contribution statement

J.F. Algorri: Conceptualization, Methodology, Software, Writing – original draft, Project administration. **V. Dmitriev:** Conceptualization, Methodology, Formal analysis, Writing – review & editing. **H.E. Hernández-Figueroa:** Writing – review & editing, Supervision, Funding acquisition. **L. Rodríguez-Cobo:** Methodology, Writing – review & editing, Funding acquisition. **F. Dell'Olio:** Methodology, Writing – review & editing, Funding acquisition. **A. Cusano:** Methodology, Writing – review & editing. **J.M. López-Higuera:** Writing – review & editing, Supervision, Funding acquisition. **D.C. Zografopoulos:** Conceptualization, Methodology, Software, Formal analysis, Writing – original draft, Writing – review & editing, Visualization, Supervision, Project administration, Funding acquisition.

Declaration of competing interest

The authors declare that they have no known competing financial interests or personal relationships that could have appeared to influence the work reported in this paper.

Data availability

Data will be made available on request.

Acknowledgments

This work was supported by the CNR-FAPESP biennial (2022–2023) bilateral project StReAM "Strongly Resonant All-dielectric Metasurfaces based on quasi-dark and toroidal modes" and by the projects PID2019-107270RB-C21, PDC2021-121172-C21 and TED2021-130378B-C21 funded by MCIN/AEI/10.13039/501100011033, FEDER and EU NextGenerationEU. J.F.A. received funding from Ministerio de Ciencia, Innovación y Universidades of Spain under Juan de la Cierva-Incorporación grant. V.D. thanks the Brazilian Agency National Council of Technological and Scientific Development (CNPq) for financial support. D.C.Z. and F.D'O. acknowledge the support of the project PRIN-2022 ALPHA "ALl-dielectric resonant metasurfaces enhancing PHoton emission phenomenA" (CUP:D53D23001060006) funded by the Italian Ministry of University and Research. H.E.H.F. acknowledges the financial support of the São Paulo Research Foundation (FAPESP), projects 2015/24517-8 (Thematic), 2021/11380-5 (CCD/CPTEn), and 2021/06506-0 (CNR Italy); and the Brazilian Council for Scientific and Technological Development (CNPq), projects 312714/2019-0 (HEHF) and 433175/2018-4 (Universal). F. D.'O acknowledges the support of the European Union under the Italian National Recovery and Resilience Plan (NRRP) of NextGenerationEU, partnership on "Telecommunications of the Future" (PE00000001 - program "RESTART").

References

[1] S. Zhang, C.L. Wong, S. Zeng, R. Bi, K. Tai, K. Dholakia, M. Olivo, Metasurfaces for biomedical applications: imaging and sensing from a nanophotonics perspective, Nanophotonics 10 (1) (2021) 259–293, http://dx.doi.org/10.1515/nanoph-2020-0373.

[2] C.-W. Qiu, T. Zhang, G. Hu, Y. Kivshar, Quo vadis, metasurfaces? Nano Lett. 21 (13) (2021) 5461–5474, http://dx.doi.org/10.1021/acs.nanolett.1c00828.

[3] V. Shvalya, G. Filipič, J. Zavašnik, I. Abdulhalim, U. Cvelbar, Surface-enhanced Raman spectroscopy for chemical and biological sensing using nanoplasmonics: The relevance of interparticle spacing and surface morphology, Appl. Phys. Rev. 7 (3) (2020) http://dx.doi.org/10.1063/5.0015246.

[4] M.I. Stockman, Nanoplasmonics: past, present, and glimpse into future, Opt. Express 19 (22) (2011) 22029–22106, http://dx.doi.org/10.1364/OE.19.022029.

[5] S.J. Barrow, X. Wei, J.S. Baldauf, A.M. Funston, P. Mulvaney, The surface plasmon modes of self-assembled gold nanocrystals, Nature Commun. 3 (1) (2012) http://dx.doi.org/10.1038/ncomms2289.

[6] J. Lu, S. Liu, S.S.E. Collins, L. Tang, X. Wei, P. Mulvaney, Fabrication of a three-dimensional plasmon ruler using an atomic force microscope, J. Phys. Chem. C 123 (32) (2019) 19871–19878, http://dx.doi.org/10.1021/acs.jpcc.9b05360.

[7] J. Yu, R. Qin, Y. Ying, M. Qiu, Q. Li, Asymmetric directional control of thermal emission, Adv. Mater. (2023) http://dx.doi.org/10.1002/adma.202302478.

[8] J.B. Khurgin, How to deal with the loss in plasmonics and metamaterials, Nat. Nanotechnol. 10 (1) (2015) 2–6, http://dx.doi.org/10.1038/nnano.2014.310.

[9] X. Wei, M. Altissimo, T.J. Davis, P. Mulvaney, Fano resonances in three-dimensional dual cut-wire pairs, Nanoscale 6 (10) (2014) 5372–5377, http://dx.doi.org/10.1039/c3nr06547b.

[10] A.I. Kuznetsov, A.E. Miroshnichenko, M.L. Brongersma, Y.S. Kivshar, B. Luk'yanchuk, Optically resonant dielectric nanostructures, Science 354 (6314) (2016) aag2472, http://dx.doi.org/10.1126/science.aag2472.

[11] D.C. Zografopoulos, O. Tsilipakos, Recent advances in strongly resonant and gradient all-dielectric metasurfaces, Mater. Adv. 4 (2023) 11–34, http://dx.doi.org/10.1039/D2MA00910B.

[12] J. Yu, B. Ma, A. Ouyang, P. Ghosh, H. Luo, A. Pattanayak, S. Kaur, M. Qiu, P. Belov, Q. Li, Dielectric super-absorbing metasurfaces via PT symmetry breaking, Optica 8 (10) (2021) 1290, http://dx.doi.org/10.1364/optica.430893.

[13] I. Al-Naib, R. Singh, C. Rockstuhl, F. Lederer, S. Delprat, D. Rocheleau, M. Chaker, T. Ozaki, R. Morandotti, Excitation of a high-q subradiant resonance mode in mirrored single-gap asymmetric split ring resonator terahertz metamaterials, Appl. Phys. Lett. 101 (7) (2012) 071108, http://dx.doi.org/10.1063/1.4745790.

[14] T.C.W. Tan, E. Plum, R. Singh, Lattice-enhanced Fano resonances from bound states in the continuum metasurfaces, Adv. Opt. Mater. 8 (6) (2020) http://dx.doi.org/10.1002/adom.201901572.

[15] J. Langer, D. Jimenez de Aberasturi, J. Aizpurua, R.A. Alvarez-Puebla, B. Auguié, J.J. Baumberg, G.C. Bazan, S.E.J. Bell, A. Boisen, A.G. Brolo, J. Choo, D. Cialla-May, V. Deckert, L. Fabris, K. Faulds, F.J. García de Abajo, R. Goodacre, D. Graham, A.J. Haes, C.L. Haynes, C. Huck, T. Itoh, M. Käll, J. Kneipp, N.A. Kotov, H. Kuang, E.C. Le Ru, H.K. Lee, J.-F. Li, X.Y. Ling, S.A. Maier, T. Mayerhöfer, M. Moskovits, K. Murakoshi, J.-M. Nam, S. Nie, Y. Ozaki, I. Pastoriza-Santos, J. Perez-Juste, J. Popp, A. Pucci, S. Reich, B. Ren, G.C. Schatz, T. Shegai, S. Schlücker, L.-L. Tay, K.G. Thomas, Z.-Q. Tian, R.P. Van Duyne, T. Vo-Dinh, Y. Wang, K.A. Willets, C. Xu, H. Xu, Y. Xu, Y.S. Yamamoto, B. Zhao, L.M. Liz-Marzán, Present and future of surface-enhanced Raman scattering, ACS Nano 14 (1) (2020) 28–117, http://dx.doi.org/10.1021/acsnano.9b04224.

[16] N. Bontempi, K.E. Chong, H.W. Orton, I. Staude, D.-Y. Choi, I. Alessandri, Y.S. Kivshar, D.N. Neshev, Highly sensitive biosensors based on all-dielectric nanoresonators, Nanoscale 9 (2017) 4972–4980, http://dx.doi.org/10.1039/C6NR07904K.

[17] O. Yavas, M. Svedendahl, P. Dobosz, V. Sanz, R. Quidant, On-a-chip biosensing based on all-dielectric nanoresonators, Nano Lett. 17 (2017) 4421–4426, http://dx.doi.org/10.1021/acs.nanolett.7b01518.

[18] A. Tittl, A. Leitis, M. Liu, F. Yesilkoy, D.-Y. Choi, D.N. Neshev, Y.S. Kivshar, H. Altug, Imaging-based molecular barcoding with pixelated dielectric metasurfaces, Science 360 (2018) 1105–1109, http://dx.doi.org/10.1126/science.aas976.

[19] Y. Jahani, E.R. Arvelo, F. Yesilkoy, K. Koshelev, C. Cianciaruso, M.D. Palma, Y. Kivshar, H. Altug, Imaging-based spectrometer-less optofluidic biosensors based on dielectric metasurfaces for detecting extracellular vesicles, Nature Commun. 12 (1) (2021) 3246, http://dx.doi.org/10.1038/s41467-021-23257-y.

[20] Y. Wang, M.A. Ali, E.K. Chow, L. Dong, M. Lu, An optofluidic metasurface for lateral flow-through detection of breast cancer biomarker, Biosens. Bioelectron. 107 (2018) 224–229, http://dx.doi.org/10.1016/j.bios.2018.02.038.

[21] B. Ma, A. Ouyang, J. Zhong, P.A. Belov, R.K. Sinha, W. Qian, P. Ghosh, Q. Li, All-dielectric metasurface for sensing microcystin-LR, Electronics 10 (11) (2021) 1363, http://dx.doi.org/10.3390/electronics10111363.

[22] H.-H. Hsiao, Y.-C. Hsu, A.-Y. Liu, J.-C. Hsieh, Y.-H. Lin, Ultrasensitive refractive index sensing based on the quasi-bound states in the continuum of all-dielectric metasurfaces, Adv. Opt. Mater. 10 (19) (2022) 202200812, http://dx.doi.org/10.1002/adom.202200812.

[23] J.F. Algorri, F. Dell'Olio, Y. Ding, F. Labbé, V. Dmitriev, J. López-Higuera, J. Sánchez-Pena, L. Andreani, M. Galli, D. Zografopoulos, Experimental demonstration of a silicon-slot quasi-bound state in the continuum in near-infrared all-dielectric metasurfaces, Opt. Laser Technol. 161 (2023) 109199, http://dx.doi.org/10.1016/j.optlastec.2023.109199.

[24] M. Caldarola, P. Albella, E. Cortes, M. Rahmani, T. Roschuk, G. Grinblat, R.F. Oulton, A.V. Bragas, S.A. Maier, Nonplasmonic nanoantennas for surface enhanced spectroscopies with ultra-low heat conversion, Nature Commun. 6 (2015) 7915, http://dx.doi.org/10.1038/ncomms8915.

[25] J. Cambiasso, M. König, E. Cortés, S. Schlücker, S.A. Maier, Surface-enhanced spectroscopies of a molecular monolayer in an all-dielectric nanoantenna, ACS Photonics 5 (2018) 1546–1557, http://dx.doi.org/10.1021/acsphotonics.7b01604.

[26] S. Romano, G. Zito, S. Managò, G. Calafiore, E. Penzo, S. Cabrini, A.C. De Luca, V. Mocella, Surface-enhanced raman and fluorescence spectroscopy with an all-dielectric metasurface, J. Phys. Chem. C 122 (34) (2018) 19738–19745, http://dx.doi.org/10.1021/acs.jpcc.8b03190.

[27] A.C. Overvig, S.C. Malek, M.J. Carter, S. Shrestha, N. Yu, Selection rules for quasibound states in the continuum, Phys. Rev. B 102 (3) (2020) http://dx.doi.org/10.1103/physrevb.102.035434.

[28] J. Kühne, J. Wang, T. Weber, L. Kühner, S.A. Maier, A. Tittl, Fabrication robustness in BIC metasurfaces, Nanophotonics 10 (17) (2021) 4305–4312, http://dx.doi.org/10.1515/nanoph-2021-0391.

[29] J. Jin, X. Yin, L. Ni, M. Soljačić, B. Zhen, C. Peng, Topologically enabled ultrahigh-q guided resonances robust to out-of-plane scattering, Nature 574 (7779) (2019) 501–504, http://dx.doi.org/10.1038/s41586-019-1664-7.

[30] W. Wang, Y.K. Srivastava, T.C. Tan, Z. Wang, R. Singh, Brillouin zone folding driven bound states in the continuum, Nature Commun. 14 (1) (2023) http://dx.doi.org/10.1038/s41467-023-38367-y.

[31] A. Sayanskiy, A.S. Kupriianov, S. Xu, P. Kapitanova, V. Dmitriev, V.V. Khardikov, V.R. Tuz, Controlling high-Q trapped modes in polarization-insensitive all-dielectric metasurfaces, Phys. Rev. B 99 (2019) 085306, http://dx.doi.org/10.1103/PhysRevB.99.085306.

[32] P. Yu, A.S. Kupriianov, V. Dmitriev, V.R. Tuz, All-dielectric metasurfaces with trapped modes: Group-theoretical description, J. Appl. Phys. 125 (14) (2019) 143101, http://dx.doi.org/10.1063/1.5087054.

[33] D.C. Zografopoulos, V. Dmitriev, Quasi-dark resonances in silicon metasurface for refractometric sensing and tunable notch filtering, J. Lightwave Technol. 39 (21) (2021) 6985–6993, http://dx.doi.org/10.1109/JLT.2021.3107953.

[34] J.F. Algorri, D.C. Zografopoulos, A. Ferraro, B. García-Cámara, R. Vergaz, R. Beccherelli, J.M. Sánchez-Pena, Anapole modes in hollow nanocuboid dielectric metasurfaces for refractometric sensing, Nanomaterials 9 (1) (2018) 30, http://dx.doi.org/10.3390/nano9010030.

[35] J.F. Algorri, D.C. Zografopoulos, A. Ferraro, B. García-Cámara, R. Beccherelli, J.M. Sánchez-Pena, Ultrahigh-quality factor resonant dielectric metasurfaces based on hollow nanocuboids, Opt. Express 27 (5) (2019) 6320–6330, http://dx.doi.org/10.1364/OE.27.006320.

[36] J. Jeong, M.D. Goldflam, S. Campione, J.L. Briscoe, P.P. Vabishchevich, J. Nogan, M.B. Sinclair, T.S. Luk, I. Brener, High quality factor toroidal resonances in dielectric metasurfaces, ACS Photonics 7 (7) (2020) 1699–1707, http://dx.doi.org/10.1021/acsphotonics.0c00179.

[37] C. Zhou, L. Huang, R. Jin, L. Xu, G. Li, M. Rahmani, X. Chen, W. Lu, A.E. Miroshnichenko, Bound states in the continuum in asymmetric dielectric metasurfaces, Laser Photonics Rev. 17 (3) (2022) 2200564, http://dx.doi.org/10.1002/lpor.202200564.

[38] Z. Liu, Y. Xu, Y. Lin, J. Xiang, T. Feng, Q. Cao, J. Li, S. Lan, J. Liu, High-Q quasibound states in the continuum for nonlinear metasurfaces, Phys. Rev. Lett. 123 (25) (2019) 253901, http://dx.doi.org/10.1103/physrevlett.123.253901.

[39] Z. Liu, J. Wang, B. Chen, Y. Wei, W. Liu, J. Liu, Giant enhancement of continuous wave second harmonic generation from few-layer GaSe coupled to high-Q quasi bound states in the continuum, Nano Lett. 21 (17) (2021) 7405–7410, http://dx.doi.org/10.1021/acs.nanolett.1c01975.

[40] M. Melli, M. West, S. Hickman, S. Dhuey, D. Lin, M. Khorasaninejad, C. Chang, S. Jolly, H. Tae, E. Poliakov, P.S. Hilaire, S. Cabrini, C. Peroz, M. Klug, Gallium phosphide optical metasurfaces for visible light applications, Sci. Rep. 10 (1) (2020) 20694, http://dx.doi.org/10.1038/s41598-020-77753-0.

[41] A.P. Anthur, H. Zhang, R. Paniagua-Dominguez, D.A. Kalashnikov, S.T. Ha, T.W.W. Maß, A.I. Kuznetsov, L. Krivitsky, Continuous wave second harmonic generation enabled by quasi-bound-states in the continuum on gallium phosphide metasurfaces, Nano Lett. 20 (12) (2020) 8745–8751, http://dx.doi.org/10.1021/acs.nanolett.0c03601.

[42] D. Khmelevskaia, D.I. Markina, V.V. Fedorov, G.A. Ermolaev, A.V. Arsenin, V.S. Volkov, A.S. Goltaev, Y.M. Zadiranov, I.A. Tzibizov, A.P. Pushkarev, A.K. Samusev, A.A. Shcherbakov, P.A. Belov, I.S. Mukhin, S.V. Makarov, Directly grown crystalline gallium phosphide on sapphire for nonlinear all-dielectric nanophotonics, Appl. Phys. Lett. 118 (20) (2021) 201101, http://dx.doi.org/10.1063/5.0048969.

[43] D.E. Aspnes, A.A. Studna, Dielectric functions and optical parameters of Si, Ge, GaP, GaAs, GaSb, InP, InAs, and InSb from 1.5 to 6.0 eV, Phys. Rev. B 27 (2) (1983) 985–1009, http://dx.doi.org/10.1103/physrevb.27.985.

[44] I.H. Malitson, Interspecimen comparison of the refractive index of fused silica, J. Opt. Soc. Amer. 55 (10) (1965) 1205, http://dx.doi.org/10.1364/josa.55.001205.

[45] C.J. Bradley, A.P. Cracknell, The Mathematical Theory of Symmetry in Solids: Representation Theory for Point Groups and Space Groups, in: Oxford Classic Texts in the Physical Sciences, Oxford University Press Inc., New York, 2009.

[46] V. Dmitriev, D.C. Zografopoulos, L.P.V. Matos, Analysis of symmetric electromagnetic components using magnetic group theory, Symmetry 15 (2) (2023) 415, http://dx.doi.org/10.3390/sym15020415.

[47] V.R. Tuz, P. Yu, V. Dmitriev, Y.S. Kivshar, Magnetic dipole ordering in resonant dielectric metasurfaces, Phys. Rev. A 13 (4) (2020) 044003, http://dx.doi.org/10.1103/physrevapplied.13.044003.

[48] D.C. Zografopoulos, J.F. Algorri, J.M. López-Higuera, H.E. Hernandez-Figueroa, V. Dmitriev, Quasi-dark resonances with antiferromagnetic order in silicon metasurfaces, Sci. Rep. 12 (1) (2022) 12975, http://dx.doi.org/10.1038/s41598-022-16167-6.

[49] P.A. Anderson, B.S. Schmidt, M. Lipson, High confinement in silicon slot waveguides with sharp bends, Opt. Express 14 (20) (2006) 9197, http://dx.doi.org/10.1364/oe.14.009197.

[50] K. Koshelev, S. Lepeshov, M. Liu, A. Bogdanov, Y. Kivshar, Asymmetric metasurfaces with high-Q resonances governed by bound states in the continuum, Phys. Rev. Lett. 121 (19) (2018) 193903, http://dx.doi.org/10.1103/physrevlett.121.193903.

[51] S. Romano, G. Zito, S.N.L. Yépez, S. Cabrini, E. Penzo, G. Coppola, I. Rendina, V. Mocellaark, Tuning the exponential sensitivity of a bound-state-in-continuum optical sensor, Opt. Express 27 (13) (2019) 18776, http://dx.doi.org/10.1364/oe.27.018776.

[52] S. Romano, G. Zito, S. Torino, G. Calafiore, E. Penzo, G. Coppola, S. Cabrini, I. Rendina, V. Mocella, Label-free sensing of ultralow-weight molecules with all-dielectric metasurfaces supporting bound states in the continuum, Photonics Res. 6 (7) (2018) 726–733.

[53] Y. Chen, C. Zhao, Y. Zhang, C. wei Qiu, Integrated molar chiral sensing based on high-q metasurface, Nano Lett. 20 (12) (2020) 8696–8703, http://dx.doi.org/10.1021/acs.nanolett.0c03506.

[54] J. Wang, J. Kühne, T. Karamanos, C. Rockstuhl, S.A. Maier, A. Tittl, All-dielectric crescent metasurface sensor driven by bound states in the continuum, Adv. Funct. Mater. 31 (46) (2021) 202104652, http://dx.doi.org/10.1002/adfm.202104652.

[55] S. Yang, M. He, C. Hong, J.D. Caldwell, J.C. Ndukaife, Engineering electromagnetic field distribution and resonance quality factor using slotted quasi-BIC metasurfaces, Nano Lett. 22 (20) (2022) 8060–8067, http://dx.doi.org/10.1021/acs.nanolett.2c01919.